Title	General Steady-State Analysis and Control Principle of Electric Springs With Active and Reactive Power Compensations
Author(s)	Tan, SC; Lee, CK; Hui, SYR
Citation	IEEE Transactions on Power Electronics, 2013, v. 28 n. 8, p. 3958-3969
Issued Date	2013
URL	http://hdl.handle.net/10722/184502
Rights	IEEE Transactions on Power Electronics. Copyright © IEEE

General Steady-State Analysis and Control Principle of Electric Springs With Active and Reactive Power Compensations

Siew-Chong Tan, *Senior Member, IEEE*, Chi Kwan Lee, *Member, IEEE*, and S. Y. (Ron) Hui, *Fellow, IEEE*

***Abstract*—This paper provides a general analysis on the steady-state behavior and control principles of a recently proposed concept of "electric springs" that can be integrated into electrical appliances to become a new generation of smart loads. The discussion here is focused on how different real and/or reactive load powers can be canceled or altered using the electric springs. Mathematical derivations supporting the theoretical framework of the concept are detailed in the paper. Experimental results validate the theoretical discussions and solutions proposed. It is demonstrated that the electric spring is capable of providing different types of power/voltage compensations to the load and the source.**

***Index Terms*—Distributed power systems, power compensation, power electronics, smart grid, smart load, stability.**

I. Introduction

With many countries worldwide determined to decarbonize electric power generation within the next few decades [1]–[3], new concerns about power system stability have arisen from the increasing use of intermittent renewable energy sources. Due to the distributed and intermittent nature of renewable energy sources, such as wind and solar energy, power companies will find it impossible to instantaneously predict and control the total power generation in the entire power grid. Future smart grid requires a new control paradigm that the load demand should follow power generation [4]–[6], which is just opposite to existing control method of power generation following load demand. Demand-side management has therefore become an important topic in smart grid research.

Recently, various methods have been proposed for demand-side management. Examples are: 1) scheduling of delay-tolerant power demand tasks [7]–[9]; 2) real-time pricing [10]–[12]; 3) use of energy storage to alleviate peak demands [13]; and 4) direct load control or on–off control of smart loads [14]–[16]. Methods 1) and 2) can be used for reducing peak load demand in predictable situation, but they are not suitable for balancing power generation and demand in real time. The energy storage method is an effective solution to reduce the difference between power generation and demand, but is considered to be an expensive option [17]. Method 4) can modulate the power demand in real time, but the on/off control of electric appliances may be intrusive to the consumer applications.

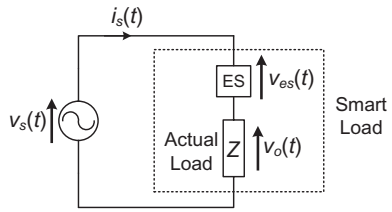

Fig. 1. Overview of an ES embedded in a smart load.

Power electronics, being an enabling technology, can offer new solutions to the stability control of future smart grid with substantial penetration of distributed and intermittent renewable energy generation. Based on the three-century old Hooke's law for mechanical springs [18], electric springs (ESs) have recently been proposed and successfully developed as a new smart grid technology for stability control in power grid and for achieving the new control paradigm of load demand following power generation. The initial concept of the ESs for reactive power compensation has been described in [19] and [20]. However, further research has indicated that the full potential of ESs has not been explored. In this paper, a steady-state analysis and control principle of ESs for both active and reactive power compensations are presented. A range of active and reactive power compensation modes for typical loads of resistive, inductive, and/or capacitive nature which ESs can support are described. These compensation modes of the ES have been practically verified with experimental prototypes.

II. ES in a Smart Load

A. Basic Principles

Fig. 1 shows an overview of the concept of smart load that comprises an ES and the actual load Z. The ES is a power electronic interface that generates an ac voltage profile $v_{es}(t)$ to act as a series compensator to modify the applied voltage of

Manuscript received July 25, 2012; revised October 18, 2012; accepted November 6, 2012. Date of current version January 18, 2013. The work of C. K. Lee and S. Y. R. Hui was supported by the Hong Kong Research Grant Council through project HKU10/CRG/10 and the University of Hong Kong for the Seed Funds through Seed Projects 201111159239 and 201203159010. Recommended for publication by Associate Editor K. Ngo.

S.-C. Tan and C. K. Lee are with the Department of Electrical and Electronic Engineering, The University of Hong Kong, Hong Kong (e-mail: sctan@eee.hku.hk; cklee@eee.hku.hk).

S. Y. R. Hui is with the Department of Electrical and Electronic Engineering, The University of Hong Kong, Hong Kong, and also with the Department of Electrical and Electronic Engineering, Imperial College London, London, SW7 2AZ, U.K. (e-mail: ronhui@eee.hku.hk).

Color versions of one or more of the figures in this paper are available online at http://ieeexplore.ieee.org.

Digital Object Identifier 10.1109/TPEL.2012.2227823

the actual load $v_o(t)$, thus directly affecting the composition of real and reactive powers flowing to the load. It can be embedded in electric appliances, forming a new generation of smart loads adaptive to the power grid. When massively distributed over the power grid, they could provide highly distributed and robust support for the smart grid, similar to the arrays of mechanical springs supporting the mattress.

The smart load is connected to an ac power source with $v_s(t)$, which may represent a strong or a weak power source on a grid network with or without transmission impedance. In this study, we adopt the general assumption that both the power source and the load are capable of bidirectional power flow, meaning that they can both act as power source (negative resistive) or power sink (resistive). The instantaneous voltage equation of this system is

$$v_s(t) = v_o(t) + v_{es}(t). \tag{1}$$

By taking $v_s(t)$ as the reference and considering only the steady-state ac-sinusoidally varying behavior of the system where $v_s(t) = \sqrt{2}|V_s|\sin(\omega t)$, the equation can be expressed as

$$|V_s|\sin(\omega t) = |V_o|\sin(\omega t + \theta_V) + |V_{es}|\sin(\omega t + \varphi_V). \tag{2}$$

Here, $|V_s|$, $|V_o|$, and $|V_{es}|$ are the root-mean-square values of $v_s(t)$, $v_o(t)$, and $v_{es}(t)$, respectively, ω is the frequency of the ac sinusoidal variation, and θ_V and φ_V are, respectively, the displacement angles of the output and ES voltages, of which

$$\begin{cases} 0 < \theta_V < +\dfrac{\pi}{2}; \quad -\dfrac{\pi}{2} < \varphi_V < 0 & \text{if load is inductive} \\ -\dfrac{\pi}{2} < \theta_V < 0; \quad 0 < \varphi_V < +\dfrac{\pi}{2} & \text{if load is capacitive} \\ \theta_V = 0; \quad \varphi_V = 0 & \text{if both load and ES are resistive} \\ \theta_V = 0; \quad \varphi_V = -\pi & \text{if load is resistive and ES is negative resistive} \\ \theta_V = -\pi; \quad \varphi_V = 0 & \text{if load is negative resistive and ES is resistive} \\ \theta_V = -\pi; \quad \varphi_V = -\pi & \text{if both load and ES are negative resistive.} \end{cases} \tag{3}$$

In the phasor form

$$|V_s|\angle 0^\circ = |V_o|\angle\theta_V + |V_{es}|\angle\varphi_V. \tag{4}$$

Since the power and load elements are connected in series, the same instantaneous current $i_s(t)$ flows through all the elements. In phasor form, the steady-state ac characteristic of this current can be written as $|I_s|\angle\theta_I$, where θ_I is the displacement angle of the current with reference to $|V_s|\angle 0^\circ$, of which

$$\begin{cases} -\dfrac{\pi}{2} \le \theta_I < 0 & \text{if source power is inductive} \\ 0 < \theta_I \le +\dfrac{\pi}{2} & \text{if source power is capacitive} \\ \theta_I = 0 & \text{if source power is resistive} \\ \theta_I = -\pi & \text{if source is negative resistive.} \end{cases} \tag{5}$$

Then, in phasor form, the steady-state ac complex power flow of the system is

$$\{\,|S_s|\angle\phi_S = |S_o|\angle\theta_S + |S_{es}|\angle\varphi_S \tag{6}$$

where $|S_s|$, $|S_o|$, and $|S_{es}|$ are the magnitudes of the complex power of the power source, the load, and the ES, respectively, and ϕ_S, θ_S, and φ_S are the displacement angles of the respective powers with reference to $|V_s|\angle 0$. Each of the these components can be expressed in terms of their voltages and currents as

$$\begin{cases} |S_s|\angle\phi_S = |V_s|\angle 0^\circ \cdot |I_s|\angle -\theta_I \\ \qquad\qquad = |V_s||I_s|\angle -\theta_I \\ |S_o|\angle\theta_S = |V_o|\angle\theta_V \cdot |I_s|\angle -\theta_I \\ \qquad\qquad = |V_o||I_s|\angle(\theta_V - \theta_I) \\ |S_{es}|\angle\varphi_S = |V_{es}|\angle\varphi_V \cdot |I_s|\angle -\theta_I \\ \qquad\qquad = |V_{es}||I_s|\angle(\varphi_V - \theta_I) \end{cases} \tag{7}$$

and they can be decomposed into their real power and reactive power components as

$$\begin{cases} |S_s|\angle\phi_S = \pm P_s \pm jQ_s \\ |S_o|\angle\theta_S = \pm P_o \pm jQ_o \\ |S_{es}|\angle\varphi_S = \pm P_{es} \pm jQ_{es} \end{cases} \tag{8}$$

where

$$\begin{cases} \pm P_s = \pm P_o \pm P_{es} \\ \pm Q_s = \pm Q_o \pm Q_{es}. \end{cases} \tag{9}$$

For a typical load Z of the following types: resistor R, resistor and inductor RL, or resistor and capacitor RC, there are eight possible types of power (voltage) compensation which the ES can support, namely:

1) inductive power ($+jQ_{es}$) compensation;
2) capacitive power ($-jQ_{es}$) compensation;
3) positive real power ($+P_{es}$) compensation;
4) negative real power ($-P_{es}$) compensation;
5) inductive plus positive real power ($+jQ_{es} + P_{es}$) compensation;
6) inductive plus negative real power ($+jQ_{es} - P_{es}$) compensation;
7) capacitive plus positive real power ($-jQ_{es} + P_{es}$) compensation;
8) capacitive plus negative real power ($-jQ_{es} - P_{es}$) compensation.

In the case of inductive power compensation, the ES emulates the characteristic of an inductor such that it has an inductive voltage drop and it introduces an inductive load power component into the system. The same analogy applies to capacitive power compensation. For positive and negative real power compensations, the ES behaves, respectively, as a positive load resistor (real power sink) that absorbs and negative load resistor (real power source) that injects real power into the system. For inductive plus positive or negative real power compensation, the ES emulates an inductor with, respectively, a positive or a negative resistor. The same analogy applies to the remaining types of power compensation. A vectorial illustration of the three power

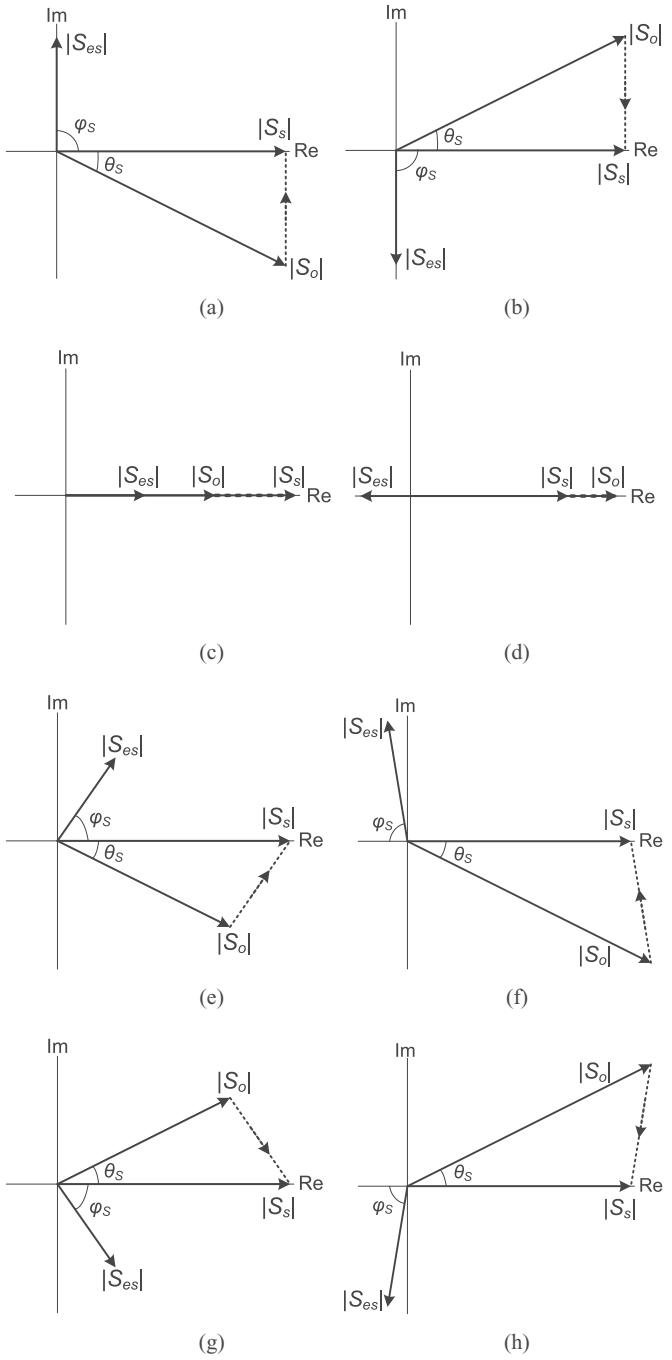

Fig. 2. Vectorial illustration of the three power quantities for different cases of power compensation. (a) Inductive, (b) capacitive, (c) positive real, (d) negative real, (e) inductive plus positive real, (f) inductive plus negative real, (g) capacitive plus positive real, and (h) capacitive plus negative real power (voltage) compensations.

quantities for the eight possible types of power compensation described previously is depicted in Fig. 2(a)–(h).

B. ES For Power and Voltage Compensations

The ES is placed between the power source and the load and it can cushion either a real ($\pm P_{es}$) and/or reactive power ($\pm jQ_{es}$) difference between the power source and the load. In doing so, power matching between source and load is possible and in terms of a power grid network, better voltage stability and regulation could be achieved. Since the same current flows through the three elements, power change is controlled by changing the voltage of ES, which will subsequently change the current and hence the power, as will be explained in the following.

Consider the circuit in Fig. 1. For any load with impedance $|Z|\angle\theta_Z = R + jX$, the real and reactive powers can be expressed as

$$\begin{cases} P_o = \dfrac{[|V_o|\cos\theta_V)]^2}{R} \\ Q_o = \dfrac{[|V_o|\sin\theta_V)]^2}{X}. \end{cases} \tag{10}$$

By considering the Euclidean of the rearrangement of (4) and substituting it into (10), we have

$$\begin{cases} P_o = \dfrac{[\|\,|V_s|\angle 0^\circ - |V_{es}|\angle\varphi_V\,\|\cos\theta_V)]^2}{R} \\ Q_o = \dfrac{[\|\,|V_s|\angle 0^\circ - |V_{es}|\angle\varphi_V\,\|\sin\theta_V)]^2}{X}. \end{cases} \tag{11}$$

As seen from the equation, both the real and reactive powers of the load are affected by $|V_{es}|$ and φ_V of the ES. On the other hand, in changing $|V_{es}|$ and φ_V, the complex power of the ES is also affected, since

$$\begin{cases} P_{es} = |V_{es}||I_s|\cos(\varphi_V - \theta_I) \\ Q_{es} = |V_{es}||I_s|\sin(\varphi_V - \theta_I). \end{cases} \tag{12}$$

This affects the overall power flow from the power source since from (9), we have

$$\begin{cases} P_s \equiv |V_s\|I_s|\cos(-\theta_I) \\ \quad = |V_o\|I_s|\cos(\theta_V - \theta_I) + |V_{es}\|I_s|\cos(\varphi_V - \theta_I) \\ Q_s \equiv |V_s\|I_s|\sin(-\theta_I) \\ \quad = |V_o\|I_s|\sin(\theta_V - \theta_I) + |V_{es}\|I_s|\sin(\varphi_V - \theta_I). \end{cases} \tag{13}$$

From the aforementioned discussion, it is obvious that the control of the power flow of each element can be equivalently performed by controlling the voltage drop across the particular element, and vice versa.

Moreover, from (13), the real power of the load is

$$\begin{aligned} P_o &= |V_o\|I_s|\cos(\theta_V - \theta_I) \\ &= |V_s\|I_s|\cos(-\theta_I) - |V_{es}\|I_s|\cos(\varphi_V - \theta_I) \end{aligned} \tag{14}$$

where

$$\begin{cases} P_o > P_s \text{ when } \cos(\varphi_V - \theta_I) = -\text{ve} \\ \qquad \text{i.e., } \dfrac{\pi}{2} < |\varphi_V - \theta_I| \le \pi \\ P_o < P_s \text{ when } \cos(\varphi_V - \theta_I) = +\text{ve} \\ \qquad \text{i.e., } 0 \le |\varphi_V - \theta_I| < \dfrac{\pi}{2} \\ P_o = P_s \text{ when } \cos(\varphi_V - \theta_I) = 0 \\ \qquad \text{i.e., } |\varphi_V - \theta_I| = \dfrac{\pi}{2} \end{cases} \tag{15}$$

and the reactive power is

$$\begin{aligned} Q_o &= |V_o\|I_s|\sin(\theta_V - \theta_I) \\ &= |V_s\|I_s|\sin(-\theta_I) - |V_{es}\|I_s|\sin(\varphi_V - \theta_I) \end{aligned} \tag{16}$$

where

$$\begin{cases} Q_o > Q_s \text{ when } \sin(\varphi_V - \theta_I) = -\text{ve} \\ \qquad \text{i.e., } -\pi < \varphi_V - \theta_I < 0 \\ Q_o < Q_s \text{ when } \sin(\varphi_V - \theta_I) = +\text{ve} \\ \qquad \text{i.e., } 0 < \varphi_V - \theta_I < \pi \\ Q_o = Q_s \text{ when } \sin(\varphi_V - \theta_I) = 0 \\ \qquad \text{i.e., } |\varphi_V - \theta_I| = 0 \text{ or } \pi. \end{cases} \tag{17}$$

Real and reactive power compensations are achievable by controlling $|V_{es}|$ and φ_V of the ES. From the equations, a change in $|V_{es}|$ or φ_V will simultaneously affect both the real and reactive power compensations. In other words, both these variables are mutually coupled to both real and reactive power compensations.

III. Steady-State Power Analysis of the ES

A. Real and Reactive Power Compensations by the ES in a Grid Delivering Only Real Power

For a grid where the power source delivers only real power, the current is in phase with the voltage. The ES described here provides reactive power compensation to cancel out the reactive power of the load $|Z|\angle\theta_Z = R + jX$ and at the same time is capable of providing positive or negative real power compensations to the load without actually changing the load impedance.

1) Real Power Compensation: Assuming that the power source is delivering only real power to the load such that $\theta_I = 0$, i.e., $Q_s = 0$, and that the load is a real power load such that $\theta_V = 0$, i.e., $Q_o = 0$, then (13) can be simplified as

$$\begin{cases} |V_s| = |V_o| + |V_{es}|\cos\varphi_V \\ \varphi_V = 0 \text{ or } \pi. \end{cases} \tag{18}$$

If $\varphi_V = 0$, then $|V_s| = |V_o| + |V_{es}|$. The real power delivered by the power source P_s is distributed between the load and the ES based on the voltage divider rule $\frac{P_{es}}{P_o} = \frac{|V_{es}|}{|V_o|}$. The ES acts as a power sink. For any desired load power $P_o < P_s$, the current and voltage of the ES can be expressed as

$$\begin{cases} |I_s|\angle\theta_I = \left|\sqrt{\dfrac{P_o}{R}}\right|\angle 0 \\ |V_{es}|\angle\varphi_V = |V_s| - |I_s|R\angle 0. \end{cases} \tag{19}$$

If $\varphi_V = \pi$, then $|V_s| + |V_{es}| = |V_o|$. The total real power of the power source and the ES is delivered to the load based on the ratio $\frac{P_{es}}{P_s} = \frac{|V_{es}|}{|V_s|}$. The ES acts as a power source. For any desired load power $P_o > P_s$, the current and voltage of the ES can be expressed as

$$\begin{cases} |I_s|\angle\theta_I = \left|\sqrt{\dfrac{P_o}{R}}\right|\angle 0 \\ |V_{es}|\angle\varphi_V = |I_s|R - |V_s|\angle\pi. \end{cases} \tag{20}$$

2) Reactive Power Compensation: Assuming that the power source is delivering only real power to the load such that $\theta_I = 0$, i.e., $Q_s = 0$, and that the reactive power of the load is fully compensated by the ES, i.e., $Q_o = -Q_{es}$, then (13) can be simplified as

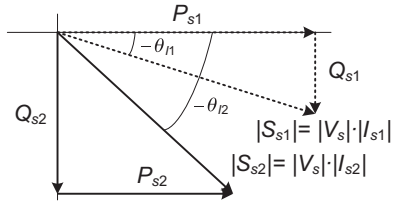

Fig. 3. Illustration of complex power compensation by the ES.

$$\begin{cases} |V_s| = |V_o|\cos\theta_V + |V_{es}|\cos\varphi_V \\ |V_{es}|\sin\varphi_V = -|V_o|\sin\theta_V. \end{cases} \tag{21}$$

Full reactive power compensation of the load by the ES is achieved when $|V_{es}|\sin\varphi_V = -|V_o|\sin\theta_V$. A pure reactive (inductive or capacitive) compensation occurs if $\varphi_V = \pm\frac{\pi}{2}$, which makes the real power component of the ES equivalent to $|V_{es}||I_s|\cos\pm\frac{\pi}{2} = 0$. In other words, the power source will deliver a real power of $P_s = |V_s||I_s|$ to the load. The ES does not draw additional real power. Here, the current and voltage of the ES is

$$\begin{cases} |I_s|\angle\theta_I = \dfrac{|V_s|}{R}\angle 0 \\ |V_{es}|\angle\theta_V = X|I_s|\angle\dfrac{\pi}{2}. \end{cases} \tag{22}$$

On the other hand, by setting a different $|V_{es}|$ and phase angle φ_V where $\varphi_V \neq \pm\frac{\pi}{2}$, reactive power compensation of the load can still be met by complying the same equation. However, since $\cos\varphi_V \neq 0$, a real power of P_{es} will either be injected into (when $\cos\varphi_V = -\text{ve}$, i.e., $\frac{\pi}{2} < |\varphi_V| \leq \pi$) or absorbed from the grid (when $\cos\varphi_V = +\text{ve}$, i.e., $0 < |\varphi_V| < \frac{\pi}{2}$) by the ES. This is the reactive plus real (complex) power compensation mentioned in the previous section. Here, the current and voltage of the ES are

$$\begin{cases} |I_s|\angle\theta_I = \frac{\left(1-\frac{P_{es}}{P_o}\right)|V_s|}{R}\angle 0 \\ |V_{es}|\angle\theta_V = \frac{\left|\sqrt{P_{es}^2+Q_{es}^2}\right|}{|I_s|}\angle\arctan\left(\dfrac{Q_{es}}{P_{es}}\right). \end{cases} \tag{23}$$

B. Real and Reactive Power Compensations by the ES in a Grid Absorbing/Delivering Complex Power

Assume that the power source is absorbing or delivering complex power from or to the load and that the ES can provide the load with real, reactive, and complex power compensations without changing the load impedance.

1) Complex Power Compensation: Fig. 3 shows the vectors of the power source for complex load power compensation where the real and reactive powers are changed from P_{s1} and Q_{s1} (without ES) to P_{s2} and Q_{s2} (with ES introducing a complex power of $P_{es} + jQ_{es}$) by adjusting the amplitude of the ES's voltage from 0 V to $|V_{es}|\angle\varphi_V$, of which the current flow changes subsequently from $|I_{s1}|\angle\theta_{I1}$ to $|I_{s2}|\angle\theta_{I2}$.

The complex power of the source without ES, which is equivalently the complex power of the load, i.e., $|S_{s1}|\angle(-\theta_{I1}) =$

$|S_{o1}|\angle(\theta_V - \theta_{I1})$, is

$$\begin{cases} P_{s1} = P_{o1} = |V_{o1}||I_{s1}|\cos(\theta_{V1} - \theta_{I1}) \\ \qquad\quad = |V_s||I_{s1}|\cos(-\theta_{I1}) \\ Q_{s2} = Q_{o1} = |V_{o1}||I_{s1}|\sin(\theta_{V1} - \theta_{I1}) \\ \qquad\quad = |V_s||I_{s1}|\sin(-\theta_{I1}) \end{cases} \tag{24}$$

where the load voltage, current, and impedance are

$$\begin{cases} |V_{o1}|\angle\theta_{V1} = |V_s|\angle 0 \\ |I_{s1}|\angle\theta_{I1} = \left|\dfrac{\sqrt{P_{s1}^2 + Q_{s1}^2}}{|V_s|}\right|\angle -\arctan\left(\dfrac{Q_{s1}}{P_{s1}}\right) \\ |Z|\angle\theta_Z = \left|\dfrac{|V_s|^2}{\sqrt{P_{s1}^2 + Q_{s1}^2}}\right|\angle\arctan\left(\dfrac{Q_{s1}}{P_{s1}}\right). \end{cases} \tag{25}$$

With the introduction of ES and without changing the load impedance, the complex power of the source is changed to $|S_{s2}|\angle(-\theta_{I2})$, where the current is

$$|I_{s2}|\angle\theta_{I2} = \left|\frac{\sqrt{P_{s2}^2 + Q_{s2}^2}}{|V_s|}\right|\angle -\arctan\left(\frac{Q_{s2}}{P_{s2}}\right). \tag{26}$$

The complex power of the load is correspondingly changed to $|S_{o2}|\angle(\theta_{V2} - \theta_{I2})$, which can be expressed as

$$\begin{cases} P_{o2} = |I_{s2}|^2|Z|\cos(\theta_Z) \\ \qquad = \left|\dfrac{P_{s2}^2 + Q_{s2}^2}{\sqrt{P_{s1}^2 + Q_{s1}^2}}\right|\cos\left[\arctan\left(\dfrac{Q_{s1}}{P_{s1}}\right)\right] \\ Q_{o2} = |I_{s2}|^2|Z|\sin(\theta_Z) \\ \qquad = \left|\dfrac{P_{s2}^2 + Q_{s2}^2}{\sqrt{P_{s1}^2 + Q_{s1}^2}}\right|\sin\left[\arctan\left(\dfrac{Q_{s1}}{P_{s1}}\right)\right] \end{cases} \tag{27}$$

where the load voltage is

$$|V_{o2}|\angle\theta_{V2} = \frac{|S_{o2}|}{|I_{s2}|}\angle(\theta_{V2} - \theta_{I2}) + \theta_{I2})$$

$$= |V_s|\left|\sqrt{\frac{P_{s2}^2 + Q_{s2}^2}{P_{s1}^2 + Q_{s1}^2}}\right|\angle\left[\arctan\left(\frac{Q_{s1}}{P_{s1}}\right) - \arctan\left(\frac{Q_{s2}}{P_{s2}}\right)\right]. \tag{28}$$

From (4), we have

$$|V_{es}|\angle\varphi_V = |V_s|\angle 0 - |V_{o2}|\angle\theta_{V2}. \tag{29}$$

Equations (28) and (29) give the solution to V_{es} and φ_V for the change of real and reactive powers of the source from P_{s1} and Q_{s1} (without ES) to P_{s2} and Q_{s2} (with ES). In this process, the ES will be introducing a complex power of $S_{es} = P_{es} + jQ_{es} = |V_{es}||I_{s2}|\angle(\varphi_V - \theta_{I2})$.

2) Real Power Compensation: Fig. 4 shows the vectors of the power source for a real power compensation operation, where the real power is changed from P_{s1} (without ES) to P_{s2} (with ES), while the reactive power Q_s is maintained constant by changing the ES's voltage from 0 V to $|V_{es}|\angle\varphi_V$.

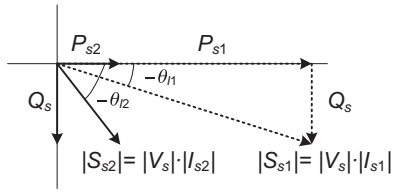

Fig. 4. Illustration of real power compensation by the ES.

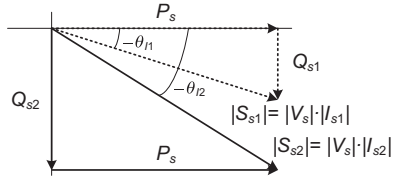

Fig. 5. Illustration of reactive power compensation by the ES.

By substituting $Q_{s1} = Q_{s2} = Q_s$ into (26) and (28), which, respectively, gives

$$|I_{s2}|\angle\theta_{I2} = \left|\frac{\sqrt{P_{s2}^2 + Q_s^2}}{|V_s|}\right|\angle -\arctan\left(\frac{Q_s}{P_{s2}}\right) \tag{30}$$

and

$$|V_{o2}|\angle\theta_{V2} = |V_s|\left|\sqrt{\frac{P_{s2}^2 + Q_s^2}{P_{s1}^2 + Q_s^2}}\right|\angle\left[\arctan\left(\frac{Q_s}{P_{s1}}\right) - \arctan\left(\frac{Q_s}{P_{s2}}\right)\right] \tag{31}$$

the solution of $V_{es}\angle\varphi_V$ can be found from (29).

3) Reactive Power Compensation: Fig. 5 shows the vectors of the power source for a reactive power compensation operation, where the reactive power is changed from Q_{s1} (without ES) to Q_{s2} (with ES), while the real power P_s is maintained constant by changing the ES's voltage from 0 V to $|V_{es}|\angle\varphi_V$.

By substituting $P_{s1} = P_{s2} = P_s$ into (26) and (28), which, respectively, gives

$$|I_{s2}|\angle\theta_{I2} = \left|\frac{\sqrt{P_s^2 + Q_{s2}^2}}{|V_s|}\right|\angle -\arctan\left(\frac{Q_{s2}}{P_s}\right) \tag{32}$$

and

$$|V_{o2}|\angle\theta_{V2} = |V_s|\left|\sqrt{\frac{P_s^2 + Q_{s2}^2}{P_s^2 + Q_{s1}^2}}\right|\angle\left[\arctan\left(\frac{Q_{s1}}{P_s}\right) - \arctan\left(\frac{Q_{s2}}{P_s}\right)\right] \tag{33}$$

the solution of $V_{es}\angle\varphi_V$ can be found from (29).

IV. Experimental Results

A. Experimental Setup

Fig. 6 shows overview of the experimental setup testing the steady-state characteristic of the ES concept in a smart load. The

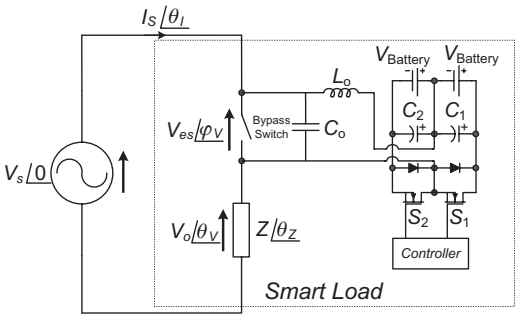

Fig. 6. Overview of the experimental setup testing the steady-state characteristic of the ES.

TABLE I
SPECIFICATIONS OF THE EXPERIMENTAL SETUP

Description	Parameter	Nominal Value
Power source	V_s	110 V_{rms}, 60 Hz
Load	Z	Resistive: 55 Ω, Inductive: $56 + j40$ Ω, Capacitive: $52 - j38$ Ω
Battery voltage	$V_{Battery}$	240 V, 5 AH lead-acid
MOSFET switches	S_1, S_2	IRFP31N50L
Storage capacitors	C_1 and C_2	3000 μF
Filter inductor	L_o	500 μH
Filter capacitor	C_o	13.2 μF
Switching frequency	f_S	20 kHz

ES adopted in this experiment is a single-phase half-bridge inverter with two sets of batteries, each 240 V, used as its dc input voltage source. With a bypassed switch connected in parallel to the inverter, the ES can be easily deactivated by turning ON the switch whenever no power/voltage compensation is needed. Here, the batteries are required for real power compensation of which when the ES operates as a positive load, the batteries are charged and as a negative load, the batteries are discharged. Alternatively, the batteries can be replaced by other types of bidirectional dc voltage source or a dc/ac bi-directional power converter of which the ac side is connected to the power grid. With this arrangement, the real power absorbed by the ES is returned to the power grid through the dc/ac bidirectional power converter and conversely real power that is released by the ES is collected from the power grid. Hence, if the control objective is to alter the overall real power consumption of the load through the storage capability of the ES, the use of a dc/ac bidirectional power converter as a replacement for battery will not be appropriate. On the other hand, if only reactive power compensation is required, as illustrated in [20], the bidirectional voltage source or storage will not be required. Here, the controller used is an NI embedded controller with SPWM control. Table I gives the specifications of the setup. Six experiments are performed to validate the various aspects of the ES's characteristics.

B. Part One—Real and Reactive Power Compensations by the ES in a Grid Delivering Only Real Power

For the experiments conducted in part one, the ES serves to provide reactive and/or real power compensations in the condition that the power source is always operating at near unit power factor (PF), i.e., the grid is providing only real power.

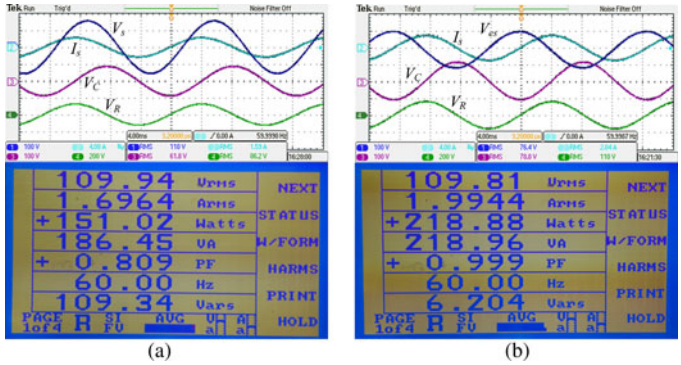

Fig. 7. Captured waveforms and data of the system with a capacitive plus resistive load of $Z = 52 - j38\ \Omega$ (a) without the ES and (b) with ES for unity power compensation.

1) Inductive Power Compensation: The objectives of this experiment are to verify the use of the ES in providing a pure inductive power compensation to the load such that the grid delivers only real power and to validate (21) and (22). From hereon, the power source used is $V_s = 110\angle 0^\circ$ V at 60 Hz. Here, the load is a capacitive plus resistive load of $Z = 52 - j38 = 64.4\angle -36.16^\circ\ \Omega$, which means that without the ES, the complex, reactive, and real powers of the load are $|S_o| = 187.9$ VA, $P_o = 151.7$ W, and $Q_o = -110.9$ VAr, respectively, and the PF is 0.807 leading.

For the case of pure inductive compensation where $\varphi_V = +\frac{\pi}{2}$, the voltage of ES can be set following (22) as

$$\begin{cases} |I_s|\angle\theta_I = \dfrac{|V_s|}{R}\angle 0 = 2\angle 0^\circ \text{A} \\ |V_{es}|\angle\theta_V = X|I_s|\angle\dfrac{\pi}{2} = 76\angle 90^\circ \text{A}. \end{cases} \tag{34}$$

This will translate (21) to

$$\begin{cases} V_R = |V_o|\cos\theta_V\angle 0 = |V_s|\angle 0^\circ \text{ V} \\ V_C = |V_o|\sin\theta_V\angle -\dfrac{\pi}{2} = 76\angle -90^\circ \text{ V}. \end{cases} \tag{35}$$

Fig. 7(a) and (b) shows the captured waveforms and data (measured using a power meter) of the system for, respectively, the operation without the ES and with the ES. From Fig. 7(a), without the ES in operation, the voltage V_s is applied entirely on the load where the current $I_s = 1.696$ A leads V_s. The voltage across the capacitive component of the load is $V_C = 64.6$ V and the resistive component is $V_R = 88.4$ V (voltages of ES and loads in all the experiments are measured using voltmeters for better accuracy). From the power meter, the reactive, real, and complex powers delivered by the power source (equivalently the power of the load) are, respectively, $P_s = P_o = 151.02$ W, $Q_s = Q_o = -109.34$ VAr, and $S_s = S_o = 186.45$ VA. The PF is 0.809 leading. This is similar to what was obtained in the calculation.

From Fig. 7(b), with the ES introducing a voltage of $V_{es} = 75.9\angle 90^\circ$ V that is in antiphase with the capacitive load voltage of $V_C = 76\angle -90^\circ$ V, the resistive load voltage is almost equivalent to the applied voltage, i.e., $V_R = 104.4$ V. The power delivered by the system is mainly of real power of $P_s = 218.88$ W and with a very small capacitive power of $Q_s = -6.20$ VAr.

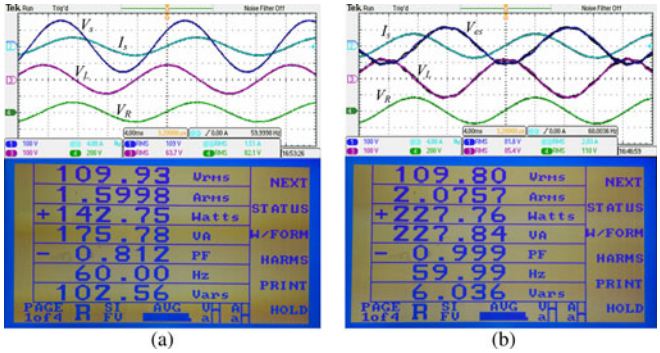

(a) (b)

Fig. 8. Captured waveforms and data of the system with an inductive plus resistive load $Z = 56 + j40\ \Omega$ (a) without the ES and (b) with ES for unity power compensation.

The PF is corrected to 0.999 leading. The real and reactive powers of the load are $P_o = \frac{V_R^2}{R} = \frac{104.4^2}{52} = 209.6$ W and $Q_o = -\frac{V_L^2}{X} = -\frac{76^2}{38} = -152$ VAr. The power of ES is mainly reactive with $Q_{es} = Q_s - Q_o = 145.8$ VAr and $P_{es} = P_s - P_o = 9.28$ W. With the ES, the current is increased to $I_s = 1.99$ A and it is in phase with V_s. The results are in good agreement with that obtained from (34) and (35).

2) Capacitive Power Compensation: In this experiment, the load is an inductive plus resistive load of $Z = 56 + j40 = 68.8\angle 35.53^\circ\ \Omega$, which means that without the ES, the complex, reactive, and real powers of the load are $|S_o| = 175.87$ VA, $P_o = 143.13$ W, and $Q_o = 102.2$ VAr, and the PF is 0.814 lagging.

For the case of pure capacitive compensation where $\varphi_V = -\frac{\pi}{2}$, the voltage of ES can be set following (22) as

$$\begin{cases} |I_s|\angle\theta_I = \dfrac{|V_s|}{R}\angle 0 = 2\angle 0^\circ \text{A} \\ |V_{es}|\angle\theta_V = X|I_s|\angle -\dfrac{\pi}{2} = 80\angle -90^\circ \text{ A}. \end{cases} \tag{36}$$

This will translate (21) to

$$\begin{cases} V_R = |V_o|\cos\theta_V\angle 0 = |V_s|\angle 0^\circ \text{V} \\ V_L = |V_o|\sin\theta_V\angle\dfrac{\pi}{2} = 80\ \angle 90^\circ \text{ V}. \end{cases} \tag{37}$$

Fig. 8(a) and (b) shows the captured waveforms and data of the system for, respectively, the operation without the ES and with the ES. From Fig. 8(a), without the ES in operation, the voltage V_s is applied entirely on the load where the current $I_s = 1.5998$ A lags V_s. The voltage across the inductive component of the load is $V_L = 64.3$ V and the resistive component is $V_R = 83.5$ V. The reactive, real, and complex powers delivered by the power source (equivalently the power of the load) are, respectively, $P_s = P_o = 142.75$ W, $Q_s = Q_o = 102.56$ VAr, and $S_s = S_o = 175.78$ VA. The PF is 0.812 lagging. This is similar to what was obtained in the calculation.

From Fig. 8(b), with the ES introducing a voltage of $V_{es} = 83.9\angle -90^\circ$ V that is in antiphase with the inductive load voltage of $V_L = 84\angle 90^\circ$ V, the resistive load voltage is almost equivalent to the applied voltage, i.e. $V_R = 108.5$ V. The power delivered by the system is mainly of real power of $P_s = 227.76$ W and with a very small inductive power of $Q_s = 6.04$ VAr. The PF is corrected to 0.999 lagging. The real and reactive powers of the load are $P_o = \frac{V_R^2}{R} = \frac{108.5^2}{56} = 210.2$ W and $Q_o = \frac{V_L^2}{X} = \frac{84^2}{40} = 176.4$. The power of ES is mainly reactive with $Q_{es} = Q_s - Q_o = -170.36$ VAr and $P_{es} = P_s - P_o = 17.07$ W. With the ES, the current is increased to $I_s = 2.076$ A and it is in phase with V_s. The results are in good agreement with that obtained from (36) and (37).

3) Resistive Power Compensation: In this experiment, the load is a resistive load of $R = 55\ \Omega$, which means that without the ES, the power of the load is $P_o = 220$ W. There are two parts in this experiment. The first part is to make the ES a power sink and to suppress the power delivered by the voltage source to $P_s = 180$ W and the second part is to make the ES a power source and to increase the power delivered by the voltage source to $P_s = 270$ W.

In the first part, with ES controlling the power at $P_s = 180$ W, the current flowing through the system is $|I_s| = \frac{P_s}{|V_s|} = 1.636$ A, which makes the load power $P_o = 147.2$ W. As $P_o < P_s$, from (19), the power and voltage of the ES can be derived as

$$\begin{cases} |V_{es}|\angle\varphi_V = |V_s| - |I_s|R\angle 0 = 20.02\angle 0^\circ \text{ V} \\ P_{es} = |I_s||V_{es}| = 32.8 \text{ W}. \end{cases} \tag{38}$$

In the second part, with ES controlling the power at $P_s = 270$ W, the current flowing through the system is $|I_s| = \frac{P_s}{|V_s|} = 2.454$ A, which makes the load power $P_o = 331.4$ W. As $P_o > P_s$, from (20), the power and voltage of the ES can be derived as

$$\begin{cases} |V_{es}|\angle\varphi_V = |I_s|R - |V_s|\angle\pi = 25\angle 180^\circ \text{ V} \\ P_{es} = |I_s||V_{es}| = -61.4 \text{ W}. \end{cases} \tag{39}$$

Fig. 9(a)–(c) shows the captured waveforms and data of the system with a resistive load of $Z = 55\ \Omega$ for, respectively, the operation without the ES and that with ES +ve real power compensation. From Fig. 9(a), without the ES in operation, the voltage V_s is applied entirely on the load of which $P_s = P_o = 220$ W. From Fig. 9(b), with the ES applied for positive compensation, the voltage source supplies a power of $P_s = 180$ W. The applied voltage of the ES is measured as $V_{es}\angle\varphi_V = 19.95\angle 0^\circ$. From Fig. 9(c), with the ES applied for negative compensation, the voltage source supplies a power of $P_s = 270$ W. The applied voltage of the ES is measured as $V_{es}\angle\varphi_V = 24.64\angle 180^\circ$. The results are in good agreement with that obtained from (38) and (39).

C. Part Two—Real and Reactive Power Compensations by the ES in a Grid Absorbing/Delivering Complex Power

In part two, the experiments are conducted without any constraint on the power source being at unit PF, i.e., the grid provides complex power.

1) Change of Reactive Power While Maintaining a Constant Real Power: In part one, it can be observed that when the reactive power compensations are performed for both capacitive and reactive cases, the real power of the load is increased [refer to Figs. 7(b) and 8(b)]. This is because when the reactive power of the load is canceled, almost the entire voltage of the power source will be applied to the resistive component of the load,

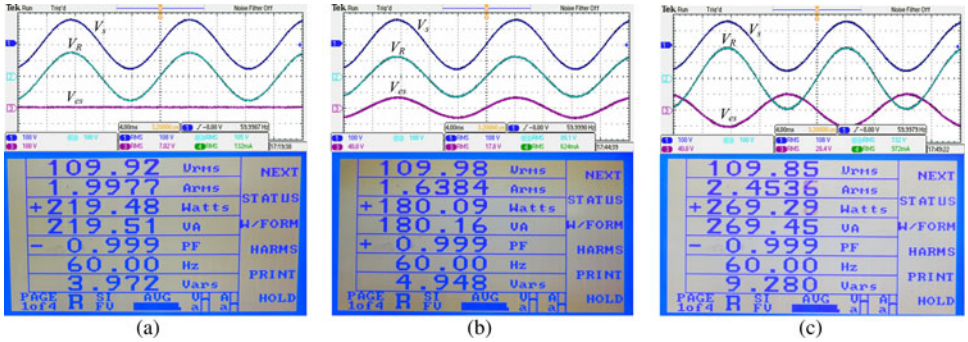

Fig. 9. Captured waveforms and data of the system with resistive load $R = 55\ \Omega$ (a) without the ES, (b) with ES of positive real power compensation, and (c) with ES of negative real power compensation.

leading to an increase in its power dissipation. In this section, an experiment is conducted to demonstrate that the change of reactive power without any change of the real power is possible with the ES. Here, the load used is an inductive plus resistive load of $Z = 56 + j40 = 68.8\angle 35.53^\circ\ \Omega$, which is similar to that described in Section IV-B2. Hence, without the ES, theoretically, $|S_s| = 175.87$ VA, $P_s = 143.13$ W, and $Q_s = 102.2$ VAr, and the PF is 0.814 lagging. The experiment conducted here shall validate that the change of PF to 0.7 and 0.9 while keeping the real power constant is achievable with, respectively, the ES producing inductive plus negative real power compensation and the ES producing capacitive plus positive real power compensation.

With PF $= 0.7$ and that $P_s = 143.13$ W, the theoretical value of the reactive power is $Q_s = 146.02$ VAr. Thus, with respect to the theoretical formulation given in Section III, $Q_{s1} = 102.2$ VAr and $Q_{s2} = 146.02$ VAr. From (32) and (33), the current and voltage of the load can be calculated as

$$|I_{s2}|\angle\theta_{I2} = \left|\frac{\sqrt{143.13^2 + 146.02^2}}{110}\right| \angle -\arctan\left(\frac{146.02}{143.13}\right) = 1.859\angle -45.57^\circ \text{A} \quad (40)$$

and

$$|V_{o2}|\angle\theta_{V2} = 110 \cdot \left|\sqrt{\frac{143.13^2 + 146.02^2}{143.13^2 + 102.2^2}}\right| \angle\left[\arctan\left(\frac{102.2}{143.13}\right) - \arctan\left(\frac{146.02}{143.13}\right)\right] = 127.89\angle -10.04^\circ \text{ V}. \quad (41)$$

From (29), the solution of $V_{es}\angle\varphi_V$ can be found as $|V_{es}|\angle\varphi_V = 27.4\angle 125.55^\circ$ V.

With PF $= 0.9$ and that $P_s = 143.13$ W, the theoretical value of the reactive power is $Q_s = 69.32$ VAr. Thus, with respect to the definition given in Section III-B3, $Q_{s1} = 102.2$ VAr and $Q_{s2} = 69.32$ VAr. From (32) and (33), the current and voltage of the load can be calculated as

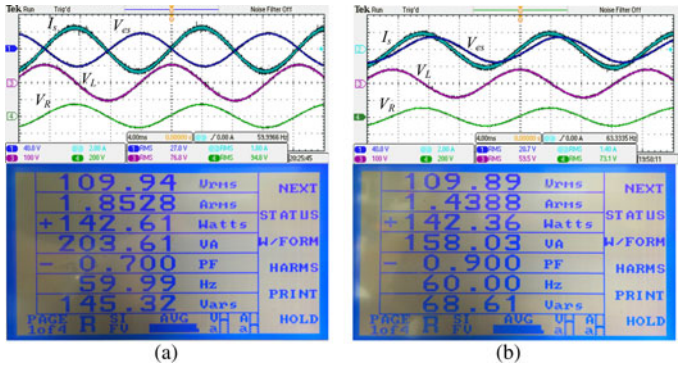

Fig. 10. Captured waveforms and data of the system with an inductive plus resistive load $Z = 56 + j40\ \Omega$ (a) with the ES correcting the PF to 0.7 and (b) with the ES correcting the PF to 0.9 both without the change of the real power. (a) PF 0.7: inductive plus $-$ve real power compensation. (b) PF 0.9: capacitive plus $+$ve real power compensation.

$$|I_{s2}|\angle\theta_{I2} = \left|\frac{\sqrt{143.13^2 + 69.32^2}}{110}\right| \angle -\arctan\left(\frac{69.32}{143.13}\right) = 1.446\angle -25.84^\circ \text{ A} \quad (42)$$

and

$$|V_{o2}|\angle\theta_{V2} = 110 \cdot \left|\sqrt{\frac{143.13^2 + 69.32^2}{143.13^2 + 102.2^2}}\right| \angle\left[\arctan\left(\frac{102.2}{143.13}\right) - \arctan\left(\frac{69.32}{143.13}\right)\right] = 99.47\angle 9.69^\circ \text{ V}. \quad (43)$$

From (29), the solution of $V_{es}\angle\varphi_V$ can be found as $|V_{es}|\angle\varphi_V = 20.57\angle -54.48^\circ$ V.

Fig. 10(a) and (b) shows the captured waveforms and data of the system for, respectively, the operation with the ES correcting the PF to 0.7 and to 0.9 lagging. Recall that without the ES [refer to Fig. 8(a)], the measured PF is 0.812 lagging and $P_s = P_o = 142.75$ W, $Q_s = Q_o = 102.56$ VAr, and $S_s = S_o = 175.78$ VA. From Fig. 10(a), with the ES introducing a voltage $V_{es} = 27.4\angle -54.45^\circ$ V (obtained from calculation), the PF is reduced to 0.7 lagging, and the reactive power is increased to $Q_s = 145.32$ VAr, while the real power is kept relatively constant at $P_s = 142.61$ W. Here, the current and

voltage values are measured as $I_s = 1.8528$ A, $V_L = 74.7$ V, $V_R = 97.4$ V, and $V_o = 127.4$ V. The results are in good agreement with that obtained from (40) and (41).

From Fig. 10(b), with the ES introducing a voltage $V_{es} = 20.57\angle -54.48^\circ$ V, the PF is increased to 0.9 lagging, and the reactive power is decreased to $Q_s = 68.61$ VAr, while the real power is kept relatively constant at $P_s = 142.61$ W. Here, the current and voltage values are measured as $I_s = 1.4388$ A, $V_L = 57.8$ V, $V_R = 75.6$ V, and $V_o = 98.7$ V. The results are in good agreement with that obtained from (42) and (43).

2) Change of Reactive Power While Maintaining a Constant Reactive Power: Conversely, a change in the real power of the system by the ES through a pure resistive power compensation will also decrease or increase the reactive power of the system if the load consists of reactive components, i.e., if PF is not unity. The objective of this experiment is to demonstrate that the change of real power without any change of the reactive power is also possible with the ES. The load used is a capacitive plus resistive load of $Z = 52 - j38 = 64.4\angle -36.16^\circ\ \Omega$, which is similar to that described in Section IV-B1. Hence, without the ES, theoretically, $|S_s| = 187.9$ VA, $P_s = 151.7$ W, and $Q_s = -110.9$ VAr, and the PF is 0.807 leading. Here, the ES will change the PF to 0.7 and 0.9 by varying the real power and keeping the reactive power constant with, respectively, a capacitive plus positive real power compensation and an inductive plus negative real power compensation.

With PF = 0.7 and that $Q_s = -110.9$ VAr, the theoretical value of the real power is $P_s = 108.7$ W. Thus, with respect to the definition given in Section III-B2, $P_{s1} = 151.7$ W and $P_{s2} = 108.7$ W. From (30) and (31), the current and voltage of the load can be calculated as

$$|I_{s2}|\angle\theta_{I2} = \left|\frac{\sqrt{108.7^2 + (-110.9)^2}}{110}\right| \angle -\arctan\left(\frac{-110.9}{108.7}\right) = 1.412\angle 45.57^\circ \text{A} \quad (44)$$

and

$$|V_{o2}|\angle\theta_{V2} = 110 \cdot \left|\sqrt{\frac{108.7^2 + (-110.9)^2}{151.7^2 + (-110.9)^2}}\right| \angle\left[\arctan\left(\frac{-110.9}{151.7}\right) - \arctan\left(\frac{-110.9}{108.7}\right)\right] = 90.9\angle 9.40^\circ \text{ V}. \quad (45)$$

From (29), the solution of $V_{es}\angle\varphi_V$ can be found as $|V_{es}|\angle\varphi_V = 25.17\angle -36.15^\circ$ V.

With PF = 0.9 and that $Q_s = -110.9$ VAr, the theoretical value of the real power is $P_s = 228.98$ W. Thus, with respect to the definition given in Section III, $P_{s1} = 151.7$ W and $P_{s2} = 228.98$ W. From (30) and (31), the current and voltage of the load can be calculated as

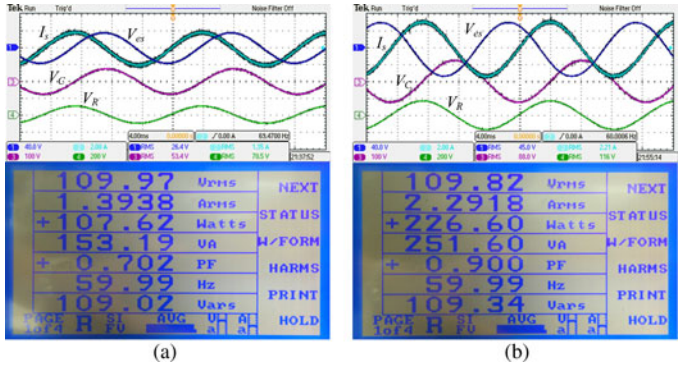

(a) (b)

Fig. 11. Captured waveforms and data of the system with a capacitive plus resistive load $Z = 52 - j38\ \Omega$ (a) with the ES correcting the PF to 0.7 and (b) with the ES correcting the PF to 0.9 both without the change of reactive power. (a) PF 0.7: capacitive plus +ve real power compensation. (b) PF 0.9: inductive plus −ve real power compensation.

$$|I_{s2}|\angle\theta_{I2} = \left|\frac{\sqrt{228.98^2 + (-110.9)^2}}{110}\right| \angle -\arctan\left(\frac{-110.9}{228.98}\right) = 2.31\angle 25.84^\circ \text{ A} \quad (46)$$

and

$$|V_{o2}|\angle\theta_{V2} = 110 \cdot \left|\sqrt{\frac{228.98^2 + (-110.9)^2}{151.7^2 + (-110.9)^2}}\right| \angle\left[\arctan\left(\frac{-110.9}{151.7}\right) - \arctan\left(\frac{-110.9}{228.98}\right)\right] = 148.93\angle -10.33^\circ \text{V}. \quad (47)$$

From (29), the solution of $V_{es}\angle\varphi_V$ can be found as $|V_{es}|\angle\varphi_V = 45.24\angle 143.82^\circ$ V.

Fig. 11(a) and (b) shows the captured waveforms and data of the system for, respectively, the operation with the ES correcting the PF to 0.7 and to 0.9 leading. Recall that without the ES [refer to 7(a)], the measured PF is 0.809 leading and $P_s = P_o = 151.02$ W, $Q_s = Q_o = -109.34$ VAr, and $S_s = S_o = 186.45$ VA. From Fig. 11(a), with the ES introducing a voltage $V_{es} = 25.17\angle -36.15^\circ$ V, the PF is reduced to 0.7 leading, and the real power is decreased to $P_s = 107.62$ W, while the reactive power is kept relatively constant at $Q_s = -109.02$ VAr. Here, the current and voltage values are measured as $I_s = 1.3938$ A, $V_L = 53.2$ V, $V_R = 72.9$ V, and $V_o = 90.3$ V. The results are in good agreement with that obtained from (44) and (45).

From Fig. 11(b), with the ES introducing a voltage $V_{es} = 45.24\angle -36.18^\circ$ V, the PF is increased to 0.9 leading, and the real power is increased to $P_s = 226.60$ W, while the reactive power is kept relatively constant at $Q_s = -109.34$ VAr. Here, the current and voltage values are measured as $I_s = 2.2918$ A, $V_L = 87.2$ V, $V_R = 119.6$ V, and $V_o = 148$ V. The results are in good agreement with that obtained from (46) and (47).

3) Change of Both Reactive and Real Powers: For the final experiment, the objective is to demonstrate that the controlled change of both reactive and real powers can be performed concurrently with the ES and to verify (28). Here, the load used is an

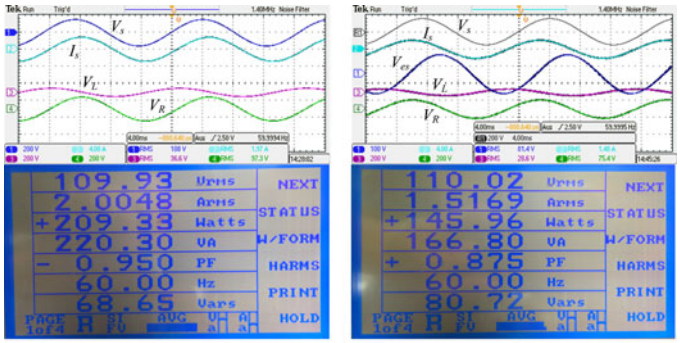

(a) (b)

Fig. 12. Captured waveforms and data of the system with an inductive plus resistive load $Z = 52 + j17\ \Omega$ (a) without the ES at PF $= 0.95$ lagging and (b) with the ES performing complex power compensation correcting the PF to 0.875 leading.

inductive plus resistive load of $Z = 52 + j17 = 54.7\angle 18.1^\circ\ \Omega$. Hence, without the ES, theoretically, $|S_s| = 221.17$ VA, $P_s = 210.23$ W, and $Q_s = 68.71$ VAr, and the PF is 0.95 lagging. The experiment conducted here shall validate that the change of real power to 145 W and reactive power to -80 VAr, i.e., PF from lagging to specifically 0.875 leading is achievable with the ES producing capacitive plus positive real power compensation. With respect to the definition given in Section III-B1, $P_{s1} = 210.23$ W, $P_{s2} = 145$ W, $Q_{s1} = 68.71$ VAr, and $Q_{s2} = -80$ VAr.

From (26) and (28), the current and voltage of the load can be calculated as

$$|I_{s2}|\angle\theta_{I2} = \left|\frac{\sqrt{145^2 + (-80)^2}}{110}\right| \angle -\arctan\left(\frac{-80}{145}\right) = 1.505\angle 28.89^\circ \text{ A} \quad (48)$$

and

$$|V_{o2}|\angle\theta_{V2} = 110 \cdot \left|\sqrt{\frac{145^2 + (-80)^2}{210.23^2 + 68.71^2}}\right| \angle\left[\arctan\left(\frac{68.71}{210.23}\right) - \arctan\left(\frac{-80}{145}\right)\right] = 82.36\angle 46.99^\circ \text{ V}. \quad (49)$$

From (29), the solution of $V_{es}\angle\varphi_V$ can be found as $|V_{es}|\angle\varphi_V = 80.77\angle -48.2^\circ$ V.

Fig. 12(a) and (b) shows the captured waveforms and data of the system for, respectively, the operation without the ES (PF $= 0.95$ lagging) and with the ES (PF $= 0.875$ leading). From Fig. 12(a), without the ES in operation, the voltage V_s is applied entirely on the load where the current $I_s = 2.0048$ A lags V_s. The voltage across the inductive component of the load is $V_L = 34.07$ V and the resistive component is $V_R = 100.4$ V. The reactive, real, and complex powers delivered by the power source (equivalently the power of the load) are, respectively, $P_s = P_o = 209.33$ W, $Q_s = Q_o = 68.65$ VAr, and $S_s = S_o = 220.3$ VA. The PF is 0.95 lagging. This is similar to what was obtained in the calculation.

TABLE II
CORE DIFFERENCES BETWEEN ESS AND SSSCS

Electric Springs	SSSC
Input voltage control for non-critical load; Output voltage control for critical load	Output voltage control
Distribution level	Transmission level
Distributed	Centralized
Transformer optional	Transformed needed
Inherent balance of power supply and demand	—-
Embedded in electric appliance	Separate equipment

From Fig. 12(b), with the ES introducing a voltage of $V_{es} = 80.77\angle -48.2^\circ$ V, the PF is changed to 0.875 leading, where the reactive power is changed to $Q_s = -80.72$ VAr and the real power is changed to $P_s = 145.95$ W. Here, the current and voltage values are measured as $I_s = 1.5169$ A, $V_L = 26.01$ V, $V_R = 77.1$ V, and $V_o = 83.8$ V. The results are in good agreement with that obtained from (42) and (43).

V. FINAL REMARKS

One may find that the operating mechanism of the ES resembles that of a static synchronous series compensator (SSSC) [21]. The SSSC is a single centralized-controlled equipment targeted at the transmission level and their control is to regulate the output voltage. The ES, on the other hand, is targeted at utilization level. The ES can be embedded in electric appliances of which each of them acts on their own in tackling voltage instability and are adaptive to the power grid. The control objective is the input voltage where the output voltage is allowed to fluctuate in the case of noncritical loads. For critical loads, the ES is controlled to regulate the output voltage, which is similar to that of the SSSC. When massively distributed over the power grid, they could provide highly distributed and robust support for the smart grid. Another major difference is that SSSC requires an output coupling transformer as they work at very high voltage. The ES discussed is at utilization voltage level. Additionally, the ES may be working at a partial portion of the voltage and not the full range of voltage. For example, if the power grid varies from 90 to 130 V of which the nominal is 110 V, an ES with ± 20 V output connected in series with a resistive load would be sufficient to regulate a critical load at 110 V throughout the power grid fluctuation. So, having a coupling transformer would be optional. The core differences between the ES and the SSSC are given in Table II.

Furthermore, by comparing ES with existing energy storage systems that also involve bidirectional converters and energy storage devices (but typically in parallel connection with the grid), the following differences are noted. For bidirectional converter-based energy storage devices, like the battery storage systems, they are typically a single large specialized system for the specific function of absorbing or releasing power from the grid to balance the power supply and demand. Connected in parallel with other loads, such energy storage systems are power buffers that will handle all the excess or shortfall powers of the power grid. In the case of the ES, being in series with the load, the power in which the ES handles will be a proportion of the

load with respect to the applied voltage of the ES. Additionally, by controlling the voltage applied to the load $\frac{v_o^2}{R}$, the ES can directly increase or decrease the load demand without actually requiring to store or release real power. In this sense, power demand and supply are balanced through demand response (increasing or decreasing the power demand of noncritical load, e.g., heater, etc.) and not solely relying on the ES to perform real power compensation in sinking or sourcing the power supply. Hence, the required energy storage in ES is relatively smaller as compared to the conventional case of simply using energy storage for balancing demand and supply. Moreover, the application of the ES is targeted at electrical appliances and at a massive widely distributed scale. In terms of reliability and redundancy, the failure of a single ES will not cause a catastrophic failure of the whole power grid.

VI. Conclusion

A general analysis on the steady-state behavior of the ES for different active and/or reactive power compensations of an ac power system is provided. Mathematical derivations supporting the theoretical framework of the concept and various control equations of the ES for the various possible types of power compensation are given. It is illustrated that for a typical load of resistive, inductive, or capacitive nature, there are eight possible types of power (voltage) compensation which the ES can support. Experimental results are in good agreement with the theoretical analysis and derivations. This is the first detailed analysis covering the fundamental principles and operating modes of the ESs. It lays down the theoretical platform for future exploration of the application potential of ESs. Based on the operating modes verified in this paper, the ESs have the application potential for voltage regulation of the load, improving power quality of the system and/or the load, frequency stabilization of power grid through real power control of a network of ESs, and for the purpose of handling unpredictable load demands.

References

[1] "Meeting the energy challenge—A white paper on energy," Department of Trade and Industry, U.K. Government, May 2007.

[2] "China eyes 20% renewable energy by 2020," China Daily, Jun. 10, 2009.

[3] "On investing in the development of low carbon technologies (SET-Plan)—A technology roadmap," Brussels, Belgium, Oct. 7, 2009.

[4] P. P Varaiya, F. F. Wu, and J. W. Bialek, "Smart operation of smart grid: Risk-limiting dispatch," *Proc. IEEE*, vol. 99, no. 1, pp. 40–57, Jan. 2011.

[5] D. Westermann and A. John, "Demand matching wind power generation with wide-area measurement and demand-side management," *IEEE Trans. Energy Convers.*, vol. 22, no. 1, pp. 145–149, Mar. 2007.

[6] P. Palensky and D. Dietrich, "Demand side management: Demand response, intelligent energy systems, and smart loads," *IEEE Trans. Ind. Inform.*, vol. 7, no. 3, pp. 381–388, Aug. 2011.

[7] A. Mohsenian-Rad, V. W. S. Wong, J. Jatskevich, R. Schober, and A. Leon-Garcia, "Autonomous demand-side management based on game-theoretic energy consumption scheduling for the future smart grid," *IEEE Trans. Smart Grid*, vol. 1, no. 3, pp. 320–331, Dec. 2010.

[8] M. Parvania and M. Fotuhi-Firuzabad, "Demand response scheduling by stochastic SCUC," *IEEE Trans. Smart Grid*, vol. 1, no. 1, pp. 89–98, Jun. 2010.

[9] M. Pedrasa, T. D. Spooner, and I. F. MacGill, "Scheduling of demand side resources using binary particle swarm optimization," *IEEE Trans. Power Syst.*, vol. 24, no. 3, pp. 1173–1181, Aug. 2009.

[10] A. J. Conejo, J. M. Morales, and L. Baringo, "Real-time demand response model," *IEEE Trans. Smart Grid*, vol. 1, no. 3, pp. 236–242, Dec. 2010.

[11] A. Mohsenian-Rad and A. Leon-Garcia, "Optimal residential load control with price prediction in real-time electricity pricing environments," *IEEE Trans. Smart Grid*, vol. 1, no. 2, pp. 120–133, Sep. 2010.

[12] A. J. Roscoe and G. Ault, "Supporting high penetrations of renewable generation via implementation of real-time electricity pricing and demand response," *IET Renewable Power Generat.*, vol. 4, no. 4, pp. 369–382, Jul. 2010.

[13] F. Kienzle, P. Ahčin, and G. Andersson, "Valuing investments in multi-energy conversion, storage, and demand-side management systems under uncertainty," *IEEE Trans. Sustainable Energy*, vol. 2, no. 2, pp. 194–202, Apr. 2011.

[14] S. C. Lee, S. J. Kim, and S. H. Kim, "Demand side management with air conditioner loads based on the queuing system model," *IEEE Trans. Power Syst.*, vol. 26, no. 2, pp. 661–668, Sep. 2010.

[15] G. C. Heffner, C. A. Goldman, and M. M. Moezzi, "Innovative approaches to verifying demand response of water heater load control," *IEEE Trans. Power Del.*, vol. 21, no. 1, pp. 388–397, Jan. 2006.

[16] A. Brooks, E. Lu, D. Reicher, C. Spirakis, and B. Weihl, "Demand dispatch," *IEEE Power Energy Mag.*, vol. 8, no. 3, pp. 20–29, May/Jun. 2010.

[17] J. L. Woodbridge, "Application of storage batteries to regulation of alternating-current systems," *Trans. Amer. Inst. Electr. Eng.*, vol. XXVII, no. 2, pp. 987–1012, 1908.

[18] R. Hooke, *De Potentia Restitutiva, or of Spring Explaining the Power of Springing Bodies,* vol. 1678. London, U.K.: John Martyn, p. 23.

[19] S. Y. R. Hui, C. K. Lee, and F. F. Wu, "Power control circuit and method for stabilizing a power supply," PCT patent application 61/389,489, Oct. 4, 2010.

[20] S. Y. R. Hui, C. K. Lee, and F. F. Wu, "Electric springs—A new smart grid technology," *IEEE Trans. Smart Grid*, vol. 3, no. 3, pp. 1552–1561, Sep. 2012.

[21] L. Gyugyi, C. D. Schauder, and K. K. Sen, "Static synchronous series compensator: A solid-state approach to the series compensation of transmission lines," *IEEE Trans. Power Del.*, vol. 12, no. 1, pp. 406–417, Jan. 1997.

Siew-Chong Tan (S'00–M'06–SM'11) received the B.Eng. (Hons.) and M.Eng. degrees in electrical and computer engineering from the National University of Singapore, Singapore, in 2000 and 2002, respectively, and the Ph.D. degree in electronic and information engineering from the Hong Kong Polytechnic University, Hong Kong, in 2005.

From October 2005 to May 2012, he was a Research Associate, Postdoctoral Fellow, Lecturer, and Assistant Professor in the Department of Electronic and Information Engineering, Hong Kong Polytechnic University, Hong Kong. From January to October 2011, he was a Senior Scientist in Agency for Science, Technology and Research (A*Star), Singapore. He is currently an Associate Professor in the Department of Electrical and Electronic Engineering, The University of Hong Kong, Hong Kong. He was a Visiting Scholar at the Grainger Center for Electric Machinery and Electromechanics, University of Illinois at Urbana-Champaign, Champaign, from September to October 2009, and an Invited Academic Visitor at the Huazhong University of Science and Technology, Wuhan, China, in December 2011. He is a coauthor of the book *Sliding Mode Control of Switching Power Converters: Techniques and Implementation* (Boca Raton, FL: CRC, 2011). His research interests are focused in the areas of power electronics and control, LED lightings, smart grids, and clean energy technologies.

Dr. Tan serves extensively as a reviewer for various IEEE/IET transactions and journals on power, electronics, circuits, and control engineering.

Chi Kwan Lee (M'08) received the B.Eng. and Ph.D. degrees in electronic engineering from the City University of Hong Kong, Kowloon, Hong Kong, in 1999 and 2004, respectively.

He was a Postdoctoral Research Fellow at the Power and Energy Research Centre, National University of Ireland, Galway, Ireland, from 2004 to 2005. In 2006, he joined the Centre of Power Electronics, City University of Hong Kong, as a Research Fellow. From 2008 to 2011, he was a Lecturer of electrical engineering at the Hong Kong Polytechnic University. He was a Visiting Academic at Imperial College London from 2010 to 2012. Since January 2012, he has been an Assistant Professor in the Department of Electrical and Electronic Engineering, The University of Hong Kong, Hong Kong. His current research interests include applications of power electronics to power systems, advanced inverters for renewable energy and smart grid applications, reactive power control for load management in renewable energy systems, wireless power transfer, energy harvesting, and planar electromagnetics for high-frequency power converters.

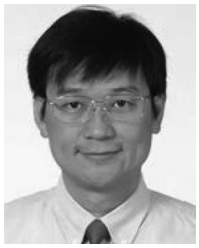

S. Y. (Ron) Hui (M'87–SM'94–F'03) received the B.Sc.Eng. (Hons.) degree from the University of Birmingham, Birmingham, U.K., in 1984, and the D.I.C. and Ph.D. degrees from Imperial College London, London, U.K., in 1987.

He has previously held academic positions at the University of Nottingham, Nottingham, U.K. from 1987 to 1990, the University of Technology, Sydney, Australia, from 1990 to 1991, the University of Sydney, Sydney, from 1992 to 1996, and the City University of Hong Kong from 1996 to 2011. He is currently the holder of the Philip Wong Wilson Wong Chair Professorship at the University of Hong Kong, Hong Kong. Since July 2010, he has been concurrently holding the Chair Professorship of power electronics at Imperial College London. He has published more than 270 technical papers, including more than 160 refereed journal publications and book chapters. More than 55 of his patents have been adopted by industry. His inventions on wireless charging platform technology underpin key dimensions of Qi, the world's first wireless power standard, with freedom of positioning and localized charging features for wireless charging of consumer electronics. He is a coinventor of electric springs.

Dr. Hui is a Fellow of the Institute of Engineering and Technology (IET). Since 1997, he has been an Associate Editor of the IEEE TRANSACTIONS ON POWER ELECTRONICS and an Associate Editor of the IEEE TRANSACTIONS ON INDUSTRIAL ELECTRONICS since 2007. He was appointed twice as an IEEE Distinguished Lecturer by the IEEE Power Electronics Society in 2004 and 2006. He served as one of the 18 Administrative Committee members of the IEEE Power Electronics Society and was the Chairman of its Constitution and Bylaws Committee from 2002 to 2010. He received the Teaching Excellence Award in 1998 and the Earth Champion Award in 2008. He won an IEEE Best Paper Award from the IEEE Industry Applications Society Committee on Production and Applications of Light in 2002, and two IEEE Power Electronics Transactions Prize Paper Awards for his publications on Wireless Charging Platform Technology in 2009 and on LED System Theory in 2010. In November 2010, he received the IEEE Rudolf Chope R&D Award from the IEEE Industrial Electronics Society, the IET Achievement Medal (The Crompton Medal), and was elected to the Fellowship of the Australian Academy of Technological Sciences and Engineering.